

---

# Deep Temporal Sets with Evidential Reinforced Attentions for Unique Behavioral Pattern Discovery

---

Anonymous Authors<sup>1</sup>

## Abstract

Machine learning-driven human behavior analysis is gaining attention in behavioral/mental health-care, due to its potential to identify behavioral patterns that cannot be recognized by traditional assessments. Real-life applications, such as digital behavioral biomarker identification, often require the discovery of complex spatiotemporal patterns in multimodal data, which is largely under-explored. To fill this gap, we propose a novel model that integrates uniquely designed Deep Temporal Sets (DTS) with Evidential Reinforced Attentions (ERA). DTS captures complex temporal relationships in the input and generates a set-based representation, while ERA captures the policy network's uncertainty and conducts evidence-aware exploration to locate attentive regions in behavioral data. Using child-computer interaction data as a testing platform, we demonstrate the effectiveness of DTS-ERA in differentiating children with Autism Spectrum Disorder and typically developing children based on sequential multimodal visual and touch behaviors. Comparisons with baseline methods show that our model achieves superior performance and has the potential to provide objective, quantitative, and precise analysis of complex human behaviors.

## 1. Introduction

Machine learning has been widely applied to detecting and analyzing human behaviors (Chen et al., 2021), with recent advances in behavioral/mental health care (Thieme et al., 2020). Digital technologies enable the collection of big and high-resolution data, which further empowered machine learning and artificial intelligence in the automated recognition of medical conditions and treatment planning

(Washington et al., 2020). However, there are still important bottlenecks. Meaningful observations of patients lead to multimodal data where complex spatiotemporal patterns are hidden and hard to catch (Cai et al., 2019). Collections of data may be incomplete and noisy, and thus lead to erroneous predictions (Le Glaz et al., 2021). In addition, health research requires a higher level of interpretability on the analytical results, making many existing models (*e.g.*, deep neural networks) unsuitable since their black-box nature cannot provide insights about the data.

To address these challenges, we propose novel integration of uniquely designed Deep Temporal Sets with Evidential Reinforced Attentions (DTS-ERA) to identify signature behavioral patterns (SBPs) based on multimodal behavioral dynamics. To evaluate the performance of the proposed model, we applied it to analyze complex spatiotemporal datasets collected from a series of computer games designed to identify the unique visual and touch behavioral patterns in response to sensory stimuli for children with Autism spectrum disorder (ASD). ASD is a prevalent (1 in 100 worldwide (Zeidan et al., 2022) and 1 in 44 in the U.S. (Maenner et al., 2021)) developmental disorder characterized by challenges in social communications as well as restricted and repetitive behaviors (APA, 2013). Human-computer interaction systems have been developed to study responsive behaviors through controlled stimuli delivery and high-resolution behavioral data collection (Bozgeyikli et al., 2017; Koirala et al., 2021), which generates important but complex spatiotemporal patterns hiding in an overwhelming amount of data points (Noel et al., 2017). In addition, users may not attend to the whole interaction, causing noises and incomplete data. Existing sequential models that process the step-wise time series data may fail to achieve satisfactory performance and extract interpretive embeddings facing these unique challenges, because the informative features and noises are weighted equally.

In the new DTS-ERA model, the DTS first extracts temporal features from the raw behavioral data and transforms the step-wise observations into a series of latent representations. Such representations can capture the sequential dependencies manifested in the various patterns of users' behaviors, which is the key to analyzing temporal data. Unlike con-

<sup>1</sup>Anonymous Institution, Anonymous City, Anonymous Region, Anonymous Country. Correspondence to: Anonymous Author <anon.email@domain.com>.

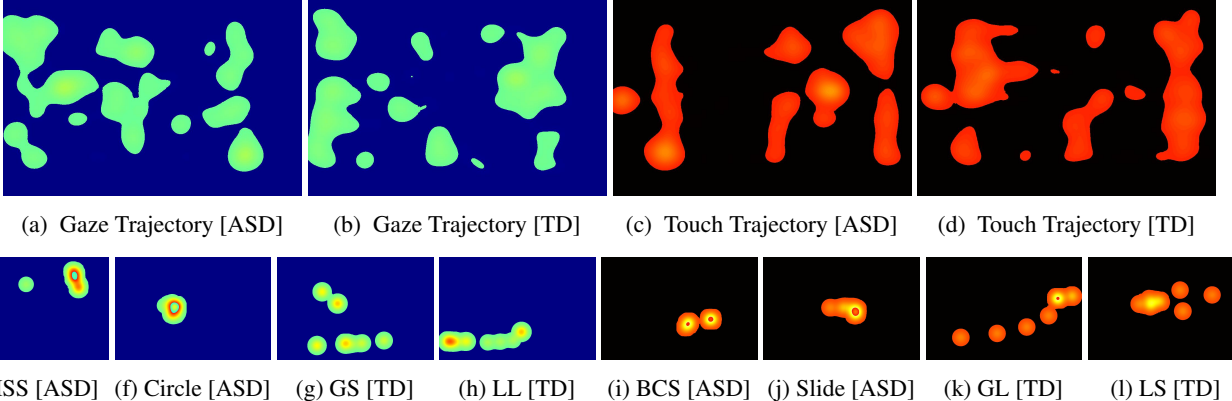


Figure 1: (a)-(d): Heatmap visualization of one ASD (ID:2) and one TD (ID:3) users’ gaze and touch trajectories; (e)-(h): signature behavioral patterns (SBPs) discovered from ASD and TD gaze trajectories, where ISS, GS, and LL stands for imbalanced scatter switching, global scan, and local line, respectively; (i)-(l) SBPs discovered from ASD and TD touch trajectories, where BCS, GL, and LS stand for balanced cluster switching, global line, and local scan, respectively.

ventional sequential models, which tend to forget early time steps, the DTS generated representation properly balances the early and recent time steps, which helps identify unusual patterns if they happen early. We further integrate DTS with evidential reinforced attentions (ERA) to perform evidence-aware exploration over DTS embeddings and attentively select and build sub-spatiotemporal sets. In particular, we introduce a uniquely designed reward function to encourage attention to the unknown but potentially important behavioral sub-sequences (called signature behavioral patterns or SBPs). The reward simultaneously considers both the prediction accuracy for exploitation and evidence-based uncertainty estimation for unknown behavior exploration. Inspired by the task formulation in few-shot learning works, we design the training objective as a sub-trajectory classification problem. DTS-ERA takes sub-trajectory data for training rather than the entire trajectory and thus is capable of processing incomplete sequential data, which is common for behavioral studies of children. As a result, informative behavioral patterns can be effectively identified (with noisy ones excluded) to ensure good interpretability along with improved predictive accuracy.

We use illustrative examples, as shown in Figure 1, to provide snapshots of experimental results and demonstrate the effectiveness of the model design. As can be seen, it is very hard to distinguish ASD and typically developing (TD) children by simply comparing their entire gaze and touch (*i.e.*, painting ball movement) trajectories as shown in Figures 1a-1d, where brightness indicates gaze duration and touch hardness, respectively. This is because the whole trajectory contains both noisy behaviors and common patterns between autistic children and their TD peers. On the other hand, Figures 1e-1l show a set of representative SBPs discovered from the ASD and TD gaze and touch trajectories, respectively by the proposed DTS-ERA model. They show clear distinctions between the ASD and TD groups

of children, which are evidenced by the thorough statistical analysis (see Table 2) conducted as part of our experiments. Meanwhile, the SBPs are highly interpretable, which unveils important behavioral differences between the two groups of users. For example, Autistic users tended to stare at fixed locations for a longer time and push or lift the painting ball with a touch sensation harder while swiping the ball less. In contrast, TD users looked around a wider area across the game board, and moved the ball in a relatively linear way, probably by following the designed painting path. Furthermore, by placing attention to these SBPs in the DTS embedding, it achieves a highly impressive classification accuracy, demonstrating the potential of using the model to facilitate behavioral phenotyping. We summarize our main contributions below:

- a novel end-to-end DTS-ERA model to analyze sparse, multimodal, dynamic, and noisy behavioral data.
- deep temporal sets to generate spatio-temporal set encoding, capable of capturing special behavioral patterns.
- evidential reinforced attentions to identify SBPs that are both discriminative and highly interpretable,
- use of task formulation to achieve accurate predictions with limited sparse information from incomplete sequences of behavioral data, making it more realistic and effective to support real-world behavioral studies.

## 2. Related Work

**Machine learning driven digital behavioral biomarker discovery.** In recent years, there has been a growing interest in identifying data-driven biomarkers leveraging machine learning techniques (Babruk et al., 2019; Bent et al., 2021; Lee et al., 2021). These biomarkers have unique advantages over traditional biomarkers such as analysis at both the individual and population level, continuous measures, and passive monitoring (Babruk et al., 2019). Lee et al. (Lee et al., 2021) leverage various machine learning ap-

proaches with putative biomarkers as an imbalance between sympathetic and parasympathetic nervous activity to predict cognitive fatigue. Further, establishing robust neuroimaging biomarkers using structural magnetic resonance imaging (MRI) with traditional machine learning mechanisms are used to diagnose and tailor treatment for ASD patients (Pagnozzi et al., 2018). In contrast to these approaches, our model is uniquely designed to capture users' signature behavioral patterns to better differentiate different user groups.

**Deep sets.** Deep Sets (DS) are a novel class of models that operate on sets (Zaheer et al., 2017). DS can handle varying input lengths and be applied to a wide range of downstream applications, including classification (Gordon et al., 2018; Gondal et al., 2021) and regression (Garnelo et al., 2018b;a). Attentive Neural Processes (ANP) (Kim et al., 2019) includes an attention-based encoder-decoder architecture and ANP-RNN (Qin et al., 2019) further extends ANP model with an RNN-based encoder structure to handle regression problems with temporal dependencies in the input. In contrast to the self-attention or cross-attention from ANP-RNN, the proposed DTS-ERA introduces novel evidential reinforced attention to select observations and build sub-spatiotemporal sets from multimodal gaze-touch trajectories. This mechanism allows the model to identify the representative SBPs in response to sensory stimuli and helps the model more accurately differentiate between the behaviors of children with ASD and those of TD.

**Reinforcement learning.** RL has been increasingly used to solve computer vision and natural language processing problems. For example, (Mnih et al., 2014) applies reinforced visual attention to recognize important image patches for digit classification. (Paulus et al., 2017) introduces a neural network model with novel intra-attention and a new training method that combines standard supervised word prediction and RL. In medical assessment, (Ye et al., 2020) proposes an RL-based synthetic sample selection method that learns to choose synthetic images containing reliable and informative features.

Our work designs a new reward function that balances classification accuracy and evidence-based exploration. Instead of performing relatively simple synthetic sample selection, we combine RL and Deep Temporal Sets (DTS) in novel ways to achieve evidential reinforced attentions to handle complex and sparse sequential multimodal data.

### 3. Preliminaries

**Data collection.** The data used for this article were collected using multiple virtual reality (VR) games (Koirala et al., 2021). While all gaming data were collected using a similar setup, where participants sat in front of a screen-based VR, the contents were quite different, including 2D and 3D Maze Painting, Word Scanning, and Coloring

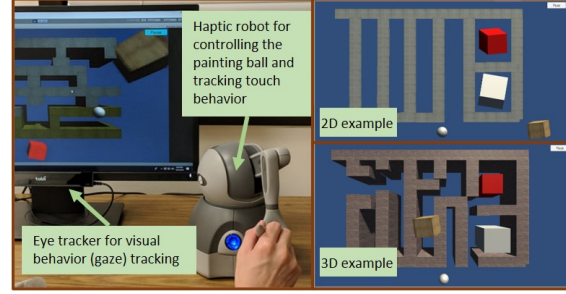


Figure 2: SAVR setup used for data collection

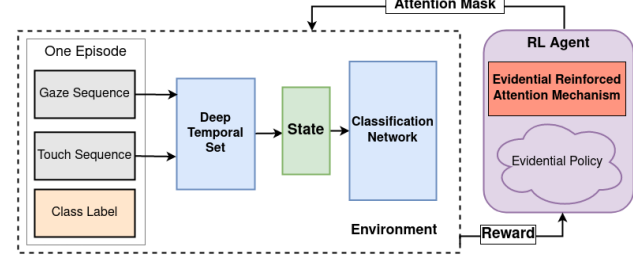


Figure 3: Overview of the proposed DTS-ERA

following a template. Figure 2 shows an example of the interface for collecting different modality data, in our case, gaze and touch, as well as Maze Painting 2D and 3D environment. Word Scanning and Coloring games were presented in a VR classroom showing on the screen, shown in Figure 14 of Appendix F. Additional details can be found in Appendix B.

**Evidential learning and uncertainty.** Evidential learning is an evidence acquisition process where every training sample adds support to learn higher order evidential distribution (Sensoy et al., 2018; Amini et al., 2020). Given the target  $y_n$ , is drawn i.i.d. from a Gaussian distribution with unknown mean and variance  $(\mu, \sigma^2)$  the model evidence can be introduced by further placing a prior distribution on  $(\mu, \sigma^2)$ . Leveraging Gaussian prior on the unknown mean and the Inverse-Gamma prior on the unknown variance, the posterior of  $(\mu, \sigma^2)$  is the Normal-Inverse-Gamma (NIG) distribution. Given a NIG posterior distribution, we can derive the mean ( $\mathbb{E}[\mu]$ ), aleatoric ( $\mathbb{E}[\sigma^2]$ ) and epistemic ( $\text{Var}[\mu]$ ) uncertainty as:

$$\mathbb{E}[\mu] = \gamma, \quad \mathbb{E}[\sigma^2] = \frac{\beta}{\alpha - 1}, \quad \text{Var}[\mu] = \frac{\beta}{\nu(\alpha - 1)} \quad (1)$$

### 4. Deep Temporal Sets with Evidential Reinforced Attentions

**Overview.** The proposed DTS-ERA model seamlessly integrates deep temporal sets with evidential reinforced attentions for signature behavioral pattern discovery from dynamic multi-modal sensory inputs. Figure 3 presents a high-level overview of the model. The DTS module extracts

165 temporal features from raw input data and transforms them  
 166 into a series of latent representations organized into a set.  
 167 Then, state representations are generated by aggregating  
 168 the DTS generated embeddings while paying special attention  
 169 to certain entries in the set, where the attended subset  
 170 is generated by an RL agent leveraging the ERA module.  
 171 ERA performs evidence-aware exploration of the DTS gen-  
 172 erated embeddings through a specially designed reward that  
 173 simultaneously considers both the prediction accuracy for  
 174 exploitation and evidence-based uncertainty estimation for  
 175 unknown behavior exploration.

#### 176 4.1. Model Design

177 We aim to develop a model  $\mathcal{F}$  that can accurately predict,  
 178 and identify the SBPs from multimodal sequential data. In  
 179 this work, we focus on SBPs that can be used to effectively  
 180 distinguish ASD and TD children given the recorded multi-  
 181 modal behavioral observations (*i.e.*, gaze and touch) during  
 182 the game-play:  
 183

$$\mathcal{F} : \{\mathbf{g}_n, \mathbf{t}_n\}_{n=1}^{N_e} \rightarrow y; \quad \mathbf{g}_n \in \mathbb{R}^{M_g}, \mathbf{t}_n \in \mathbb{R}^{M_t} \quad (2)$$

184 where  $y \in [0, 1]$ ,  $\mathcal{T} = \{\mathbf{g}_n, \mathbf{t}_n\}_{n=1}^{N_e}$  represents the entire  
 185 data within an episode (*a.k.a.*, trajectory). In this trajectory,  
 186  $(\mathbf{g}_n, \mathbf{t}_n)$  represents  $n^{\text{th}}$  instance and  $N_e$  is the number of  
 187 gaze and touch data points in the episode. Each gaze feature  
 188 is  $M_g$  dimensional, each touch feature is  $M_t$  dimensional,  
 189  $y = 1$  represents an ASD user, and  $y = 0$  is a TD user. The  
 190 length of trajectory  $N_e$  varies across the users and episodes.  
 191

192 Inspired by the task formulation in few-shot learning (Gar-  
 193 neleno et al., 2018a; Gordon et al., 2018), we design the  
 194 training objective as a sub-trajectory classification prob-  
 195 lem. Specifically, we randomly sample a sub-trajectory  
 196  $\mathcal{T}^s = \{\mathbf{g}_n, \mathbf{t}_n\}_{n=k}^{k+N_s}$  of length  $N_s$  ( $\forall k \in [1, N_e - N_s]$ ) from  
 197 the trajectory  $\mathcal{T}$  (ignoring padding  $3p$  for simplicity) and  
 198 train the model to accurately identify the user group based  
 199 on the limited sub-trajectory information (*i.e.*,  $\mathcal{F} : \mathcal{T}^s \rightarrow y$ ).  
 200 This addresses the limited data problem, enables the model  
 201 to train on a large number of training tasks, and encourages  
 202 the model to capture multiple identifying patterns of users.  
 203 Moreover, this sub-trajectory-based classification is likely  
 204 to be more realistic and representative in real-world settings  
 205 especially involving children. Simply, children are likely  
 206 to paint a maze in multiple rounds and in each round, fo-  
 207 cuses on painting for a couple of seconds (a sub-trajectory  
 208 or sequence) instead of a single round of painting. Some  
 209 children may not even complete the game and we may only  
 210 have partial trajectory information available.  
 211

212 **Deep Temporal Sets (DTS).** DTS, as shown in Figure 4,  
 213 consists of a temporal encoder  $\Phi_t$  which encodes each em-  
 214 bedding using all past sequence information and a spatial  
 215 encoder  $\Phi_s$  which generates embedding by considering  
 216 nearby local information in the sequence. Note that we  
 217 apply separate sequence encoders for different modalities  
 218

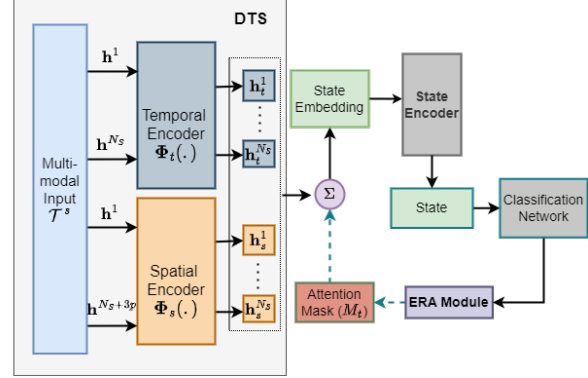


Figure 4: Architecture of Deep Temporal Sets (DTS)

(e.g., gaze and touch) in the implementation to fully leverage the multimodal information. The multimodal inputs are passed through temporal (e.g., LSTM or GRU networks) and spatial encoders (e.g., FCN) to capture the past and local information from the sequence and generate the encoding  $\mathbf{h}_t^k$  and  $\mathbf{h}_s^k$ , respectively,  $\forall k \in [1, N_s]$ , where each encoding matches with the original instance in the input sequence  $\mathcal{T}^s$ . We instantiate the spatial encoder with the FCN network using three Convolution-1D blocks with kernel size  $p$ , thus requiring a longer sequence with size  $N_s + 3p$  as input by considering future  $p$  instances as padding in each block. Each encoding can be seen as the representation for the multimodal sequential input around time step  $k$ . Then, those deep-set encodings output by different sequence encoders are concatenated and aggregated through an average pooling operation to obtain the deep-set encoding  $\mathbf{d}$ :

$$\begin{aligned} \mathbf{d} &= \text{DTS}([\mathbf{h}^1, \dots, \mathbf{h}^{N_s}]) \\ &= \frac{1}{N_s} \sum_{i=1}^{N_s} \text{concat}[\Phi_t(\mathbf{h}^i), \Phi_s(\mathbf{h}^i)] \end{aligned} \quad (3)$$

Here,  $\text{concat}$  is a concatenation function. The deep-set encoding operation for the multimodal sequential inputs is permutation invariant, *i.e.*, for any permutation  $P$ :

$$\text{DTS}([\mathbf{h}^1, \dots, \mathbf{h}^{N_s}]) = \text{DTS}([\mathbf{h}^{P(1)}, \dots, \mathbf{h}^{P(N_s)}]) \quad (4)$$

This design can be seen as a multimodal realization of deep sets encoder of (Zaheer et al., 2017) that takes the form  $f(X) = \rho(\sum_{x \in X} \phi(x))$  where  $\phi$  is the sequence encoder, and  $\rho$  is the mean aggregation function.

**Evidential Reinforced Attentions (ERA).** In ERA (shown in Figure 5), we first construct the current state embedding  $(\mathbf{e}_t)$  by concatenating the DTS generated embedding  $\mathbf{d}$  and the RL-agent selected attentive subset embedding  $\mathbf{d}_{attn}^t$ :

$$\mathbf{e}_t = \text{concat}(\mathbf{d}, \mathbf{d}_{attn}^t) \quad (5)$$

We leverage a state encoder (SE), which takes the current state embedding  $(\mathbf{e}_t)$  and previous state  $(\mathbf{s}_{t-1})$  to generate

220 current state-space ( $\mathbf{s}_t$ ) as:

$$\mathbf{s}_t = \text{SE}(\mathbf{e}_t, \mathbf{s}_{t-1}; \theta_{se}) \quad (6)$$

221  
222 We develop an evidential policy network ( $\pi_{\theta_e}$ ) parameterized by  $\theta_e$ , which takes the  $\mathbf{s}_t$  as an input and output evidential distribution parameters ( $\gamma, \nu, \alpha, \beta$ ), where the meanings  
223  
224 of these parameters are given in Section 3. Then, the likelihood of choosing an action,  $\mathbf{a}_t$  is obtained by marginalizing  
225 over the prior parameters ( $\mu, \sigma^2$ ):  
226  
227  
228  
229

$$\begin{aligned} p(\mathbf{a}_t | \gamma, \nu, \alpha, \beta) \\ = \int_{\sigma^2} \int_{\mu} p(\mathbf{a}_t | \mu, \sigma^2) p(\mu, \sigma^2 | \gamma, \nu, \alpha, \beta) d\mu d\sigma^2 \\ = \text{St}(\mathbf{a}_t; \gamma, \beta(1 + \nu) / (\nu\alpha), 2\alpha) \end{aligned} \quad (7)$$

230  
231 where  $\text{St}(\mathbf{a}_t; \gamma, \beta(1 + \nu) / (\nu\alpha), 2\alpha)$  is the Student-t distribution  
232 with location, scale, and degrees of freedom respectively,  
233 which is achieved by placing a NIG evidential prior  
234 on a Gaussian likelihood.  
235

236 From this Student-t distribution, we sample an action  $\mathbf{a}_t$   
237 that provides the attentive location in DTS and directs the  
238 policy update, respectively. It should be noted that our  
239 action is a continuous vector of length  $N_a$  representing all  
240 the starting position of an attention window. Specifically, for  
241 each attention  $a_t^k$  ( $k \in [1, N_a]$ ), we apply a sigmoid function  
242 ( $\sigma$ ) and multiply it with length of  $(N_s - W)$ , where  $W$   
243 represents the size of attention window. We then generate  
244 the attention starting index using a floor function:  
245  
246

$$idx_t^k = \lfloor \sigma(a_t^k) \cdot (N_s - W) \rfloor \quad (8)$$

247 We construct an all-zero mask  $M_t$  of length  $N_s$  and then flip  
248 the entries indexing in  $[idx_t^k, idx_t^k + W], \forall k \in [1, N_a]$  to  
249 1. The RL selected attentive subset embedding in time step  
250  $t$   $\mathbf{d}_{attn}^t$  is then obtained by  $M_t \cdot \text{concat}(\Phi_t(\mathbf{h}^i), \Phi_s(\mathbf{h}^i))$ ,  
251 where  $\cdot$  symbolizes dot product function.  
252

253 We design a novel evidential reward function that incorpo-  
254 rates standard RL reward computed with predicted classi-  
255 fication accuracy and epistemic uncertainty that captures  
256 policy network's uncertainty while providing an action:  
257  
258

$$\begin{aligned} r^e(\mathbf{s}_t, \mathbf{a}_t) &= r(\mathbf{s}_t, \mathbf{a}_t) + \lambda \text{epistemic}(\pi_{\theta_e}(\cdot | \mathbf{s}_t)) \\ r(\mathbf{s}_t, \mathbf{a}_t) &= \mathbb{1}\{p_T = y_s\} \end{aligned} \quad (9)$$

259 where  $r(\mathbf{s}_t, \mathbf{a}_t)$  is a predictive reward representing the  
260 classification accuracy at last time step  $T$ ,  $p_T$  is the  
261 last time step's predicted result while  $y_s$  is the user  
262 category label corresponding to sub trajectory  $\mathcal{T}^s$ , and  
263  $\text{epistemic}(\pi_{\theta_e}(\cdot | \mathbf{s}_t)) = \text{Var}[\mu] = \frac{\beta}{\nu(\alpha-1)}$  is the epis-  
264 temic uncertainty.  
265

266 Given the evidential reward, we introduce an epistemic value  
267 function,  $V^e(\mathbf{s}_t)$ , which can be computed by repeatedly  
268  
269  
270  
271

272 applying the Bellman operator ( $B^\pi$ ):  
273  
274

$$B^\pi V^e(\mathbf{s}_t) \triangleq r^e(\mathbf{s}_t, \mathbf{a}_t) + \gamma_{RL} \mathbb{E}_{\mathbf{s}_{t+1} \sim \pi}[V(\mathbf{s}_{t+1})] \quad (10)$$

275 The detailed workflow of the ERA module is presented in  
276 Figure 5. The module takes  $\mathbf{s}_t$  as input to the evidential  
277 policy network that generates evidential distribution parame-  
278 terers. We further marginalize those parameters and achieve  
279 a predictive student-t distribution and from which we sam-  
280 ple an action  $\mathbf{a}_t$ . We generate attention masks based on the  
281 provided action and then select attentive gaze and touch  
282 embeddings and compute evidential reward simultaneously.  
283  
284

## 4.2. Derivation of Epistemic Policy Iteration

We derive epistemic policy iteration to achieve optimal policy by alternating between epistemic policy evaluation and epistemic policy improvement.

**Lemma 1** (Epistemic Policy Evaluation). *Given the Bellman operator  $B^\pi$  in (10) and  $V^{n+1} = B^\pi V^n$ , the value will converge to the epistemic value of policy  $\pi$  as  $n \rightarrow \infty$ .*

**Lemma 2** (Epistemic Policy Improvement). *Given a new policy  $\pi_{new}$  that is updated via (15), then  $V_{\pi_{new}}^e(\mathbf{s}_t) \geq V_{\pi_{old}}^e(\mathbf{s}_t)$  for all  $\mathbf{s}_t$ .*

**Theorem 3** (Epistemic Policy Iteration). *Alternating between epistemic policy evaluation and epistemic policy improvement for any policy  $\pi \in \Pi$  converges to an optimum epistemic policy  $\pi^*$  such that  $V^{\pi^*}(\mathbf{s}_t) \geq V_\pi^e(\mathbf{s}_t)$  for all  $\mathbf{s}_t$ .*

Please refer to Appendices D.1, D.2 and D.3 for proofs.

## 4.3. Training and Inference

The training procedure involves the parameter update associated with both DTS and ERA modules. The DTS module is trained with supervised learning utilizing binary cross-entropy loss as:

$$\begin{aligned} \mathcal{L}(\theta_d, \theta_{NN}) \\ = -\frac{1}{T} \sum_{t=1}^T y_s \cdot \log(\text{NN}(\mathbf{s}_t)) + (1 - y_s) \cdot \log(1 - \text{NN}(\mathbf{s}_t)) \end{aligned} \quad (11)$$

where NN is a binary classifier neural network, and  $y_s$  is a ground truth label. Then the DTS module is updated as:

$$\theta_d \leftarrow \theta_d - \eta_d \nabla_{\theta_d} \mathcal{L}(\theta_d, \theta_{NN}) \quad (12)$$

Also, the classification network is updated as:

$$\theta_{NN} \leftarrow \theta_{NN} - \eta_{NN} \nabla_{\theta_{NN}} \mathcal{L}(\theta_d, \theta_{NN}) \quad (13)$$

Similarly, the ERA module finds the optimal policy to maximize long-term expected cumulative evidential reward as:

$$J_\pi(\theta_e) = \sum_{t=1}^T \mathbb{E}_{(\mathbf{s}_t, \mathbf{a}_t) \sim \pi}(r_\pi^e(\mathbf{s}_t, \mathbf{a}_t)) \quad (14)$$

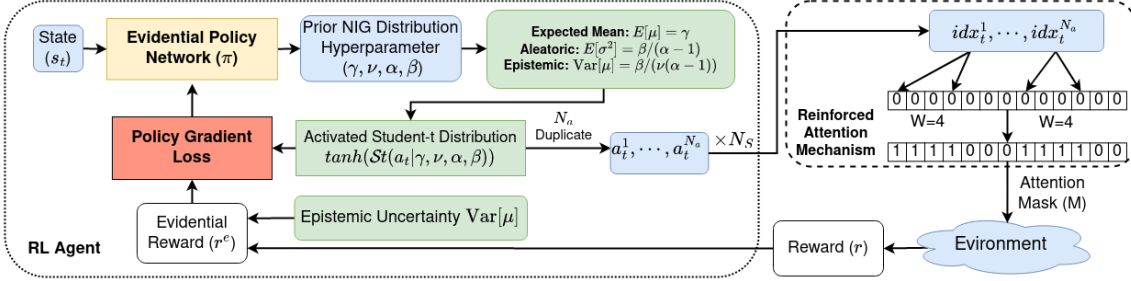


Figure 5: Evidential Reinforced Attentions (ERA)

where  $T$  is the total number of time steps in the episode.

For ERA module update, we update the evidential policy network with policy gradient method:

$$\theta_e \leftarrow \theta_e + \eta_e \nabla_{\theta_e} J_\pi(\theta_e) \quad (15)$$

where  $\nabla_{\theta_e} J_\pi(\theta_e)$  is proportion to

$$\mathbb{E}_{(\mathbf{s}_t, \mathbf{a}_t) \sim \pi} [r_\pi^e(\mathbf{s}_t, \mathbf{a}_t) \nabla_{\theta_e} \ln \text{St}(\mathbf{a}_t; \pi_{\theta_e}(\cdot | \mathbf{s}_t))]$$

The detailed training process is given in Algorithm 1 of Appendix C. During inference, we input the model with variable length sub-trajectories or full episode trajectories to test the model's capability in classifying the provided trajectory belonging to ASD or TD users. We provide details of the inference process in the experimental section.

## 5. Experiments

In this section, we conduct both quantitative and qualitative experiments to evaluate the proposed DTS-ERA model on three different games regarding ASD detection, Maze Painting, Word Scanning and Coloring. First, we compare our model with multiple state-of-the-art baselines. The performance comparison shows that our model surpasses all the competitors by a significant margin. Next, we use Maze task as an example and conduct a detailed ablation study to test the reinforced attention and evidential learning's effectiveness w.r.t. the final classification performance. We then demonstrate the model's capability in detecting ASD users' unique behaviors using incomplete gameplay trajectories. For qualitative studies, we show representative SBPs discovered from ASD and TD groups' touch and visual sensory inputs and formally group these SBPs into four major categories. We further conduct a statistical analysis to show that ASD and TD groups of children exhibit a clear distinction on certain SBPs through the Wilcoxon rank sum test.

**Dataset Setup.** All data collection experiments are approved by Institutional Review Boards and conducted under informed consent and minor assent (IRB# and institute names are hidden for review). All participants are adolescents (age 11-17 years), and all data are completely deidentified. The Maze Painting experiments are carried out

with 12 TD children and 12 children with ASD. All participants are seated in front of a screen and played 12 interactive game levels, 6 with 2D mazes and 6 with 3D mazes. The Word Scanning and Coloring experiments are conducted with 9 children with ASD and 13 TD children. More details about the experiments are in Appendix B.

**Comparison baselines.** We compare with multiple state-of-the-art baselines, all of which are trained using the same sub-trajectory-based task formulation:

- **Recurrent Classifier (LSTM)** (Hochreiter & Schmidhuber, 1997): We consider a LSTM based classifier as a simple recurrent based baseline that leverages the multimodal sequential information for classification. The model uses two sequence encoders to generate the task representation. Specifically, the output from the final time step is concatenated to obtain the task representation.
- **LSTM-FCN** (Karim et al., 2017): LSTM-FCN explores the augmentation of fully convolutional networks with LSTM RNN sub-modules for time series classification.
- **GRU-FCN** (Elsayed et al., 2018): GRU-FCN replaces LSTM with a gated recurrent unit (GRU) to create a GRU-fully convolutional network hybrid model.
- **1D-ResCNN** (ResCNN) (Zou et al., 2019): ResCNN integrates residual network with convolutional neural network for time series classification.
- **Temporal Convolutional Networks (TCN)**: (Bai et al., 2018) TCN extends convolutional neural networks for sequence modeling by introducing dilated, causal convolutional networks for sequential time-series classification.
- **InceptionTime** (Ismail Fawaz et al., 2020): Inception-Time is a scalable model that utilizes cascade of inception modules for multivariate time series classification.
- **MiniRocket**: (Dempster et al., 2021): MiniRocket transforms input using a fixed set of convolutional kernels and trains a linear classifier using the transformed features.
- **An Explainable Convolutional Neural Network (XCM)** (Fauvel et al., 2021): XCM is a new compact convolutional neural network which extracts information relative to the observed variables and time directly from the input data. Thus, XCM architecture enables a good generalization ability on both large and small datasets.

330  
 331  
**5.1. Quantitative Results**  
 332  
**Classification performance.** We compare DTS-ERA’s  
 333 predictive accuracy with the baselines on the 2D, 3D and  
 334 mixed (including both 2D and 3D ) game data for Maze  
 335 Painting as well as the other two games in Table 1. As  
 336 can be seen, DTS-ERA outperforms all baselines by a signif-  
 337 icant margin. Working across all these real-world datasets  
 338 further demonstrates our model’s generalization capability  
 339 in human behavior analysis. For component analysis, the  
 340 basic LSTM model’s performance is considerably low as it  
 341 only looks at the long and short-term temporal structure and  
 342 fails to capture the representative patterns of autistic users.  
 343 XCM baseline extracts the complex relationship relative  
 344 to the observed variables from the input data but fails to  
 345 leverage the long and short temporal information as LSTM.  
 346 MiniRocket uses fixed convolutional kernels to obtain the  
 347 features, and uses a linear classifier for prediction. TCN and  
 348 InceptionTime models extend the conventional CNN  
 349 modules for time series data leading to improved classi-  
 350 fication performance. The DTS baseline shows that even  
 351 without ERA, our model is stronger than all its competitors  
 352 by leveraging deep temporal set construction. However, all  
 353 models lack the novel reinforced attention mechanism to  
 354 identify the most characteristic behavioral patterns to distin-  
 355 guish ASD from TD. The reinforced attention mechanism  
 356 enables our model to identify the SBP leading to superior  
 357 classification performance.

358  
**359 Handling Incomplete Trajectories.** Our model can easily  
 360 be extended to handle situations with partial and incomplete  
 361 data because our model is a novel extension to the deep  
 362 sets methods. We test our model’s capability in adapting  
 363 to different length partial trajectory up to the entire episode  
 364 to match the real cases, where data recording might be par-  
 365 tially missing or interrupted. As Figure 6a and 6b show, we  
 366 use game Maze Painting as an example and our model  
 367 could achieve up to 85% test classification accuracy as the  
 368 test trajectory going to completion, and already achieves  
 369 more than 65% accuracy even with only 1/5 completion  
 370 degree, either in 2D and 3D dataset. Please refer to Appendix  
 371 E for additional partial trajectory experimental results on  
 372 the mixed dataset.

## 373 5.2. Ablation Study

374 We conduct an ablation study with game Maze  
 375 Painting to evaluate two uniquely designed components  
 376 in our model: epistemic uncertainty and evidential rein-  
 377 forced attentions. As shown in Figure 7a, ERA helps our  
 378 model identify important SBPs and improve classification  
 379 accuracy. As shown in Figure 7b, evidential uncertainty-  
 380 based exploration could help our model identify more di-  
 381 verse patterns from long-term multi-modal data. In addition,  
 382 Table 2 discloses the newly identified pattern category (in  
 383 bold font), which supports the effectiveness of the evidential  
 384 uncertainty-based exploration. Additional ablation studies

on other hyper-parameters are presented in Appendix E.

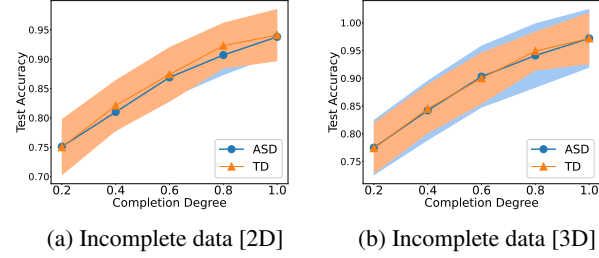


Figure 6: Predictive accuracy for incomplete episodes

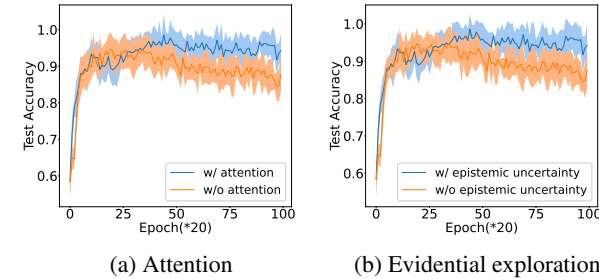


Figure 7: Average performance w/ and w/o reinforced attention mechanism (a) and evidential exploration (b).

## 5.3. Qualitative Results

**Signature Behavioral Patterns.** We continue using Maze Painting as an illustrative example. Through the reinforced attention mechanism, the RL agent is able to focus on a subset of instances to formulate the state embedding. We find that these selected instances reveal different gaze and touch modality patterns for different user groups, and therefore they can be considered both representative and discriminative. We visualize those patterns using the heatmaps in Figure 8. Each point’s location in the heatmap corresponds to a 2-dimensional feature (e.g., the coordinates of the eye gaze position and the ball position on the screen). The brightness corresponds to the gaze lasting time (eye gaze) or pressure on the ball (touch) around that position.

In Figure 9, we show the statistical counts for each sensory group’s SBPs. From those results, we observe that the ASD group presents more patterns than TD in concentrated gaze patterns (Shift, Oval, Circle) and Switching gaze patterns (BCS, BSS, ICS, ISS), while the TD group reveals more patterns than ASD in local, global and line shape patterns (LS, GS, LL). We further apply a Wilcoxon rank sum test to evaluate if the pattern differences in the two user groups are statistically significant. Here  $p < 0.05$  is considered significant (with 95% confidence), while  $0.05 \leq p < 0.1$  is considered near significant.

Table 2 shows the p-value for each pattern category (the pattern category with a bold font is the sensory pattern detected by the reinforced attention mechanism). From those

Table 1: Classification Performance Comparison

Dataset	Maze-2D	Maze-3D	Maze-Mixed	Coloring	Word Scanning
LSTM (Hochreiter & Schmidhuber, 1997)	65.0±6.7	63.0±5.5	68.8±4.8	62.0±3.8	62.5±4.1
LSTM-FCN (Karim et al., 2017)	91.5±3.6	93.4±3.5	90.4±3.8	86.0±4.2	89.0±4.1
TCN (Bai et al., 2018)	73.1±4.5	64.0±7.1	60.5±5.7	64.0±4.1	68.0±3.7
GRU-FCN (Elsayed et al., 2018)	92.3±3.2	94.5±4.1	91.8±4.8	88.0±3.9	91.0±3.8
ResCNN (Zou et al., 2019)	85.0±5.2	76.0±4.5	82.0±6.2	85.0±4.3	88.0±4.2
InceptionTime (Ismail Fawaz et al., 2020)	80.1±6.7	72.5±1.6	78.8±4.8	82.0±4.1	77.0±4.2
XCM (Fauvel et al., 2020)	37.5±3.7	44.4±4.3	54.40±3.6	58.0±3.6	52.0±4.2
MiniRocket (Dempster et al., 2021)	70.7±7.1	55.3±3.5	56.3±3.8	65.0±4.8	65.0±5.1
DTS	93.1±3.6	94.6±5.8	92.7±5.6	89.0±4.5	92.5±4.4
<b>DTS-ERA</b>	<b>94.0±3.8</b>	<b>95.3±5.3</b>	<b>95.0±5.2</b>	<b>91.0±3.9</b>	<b>93.5±3.8</b>

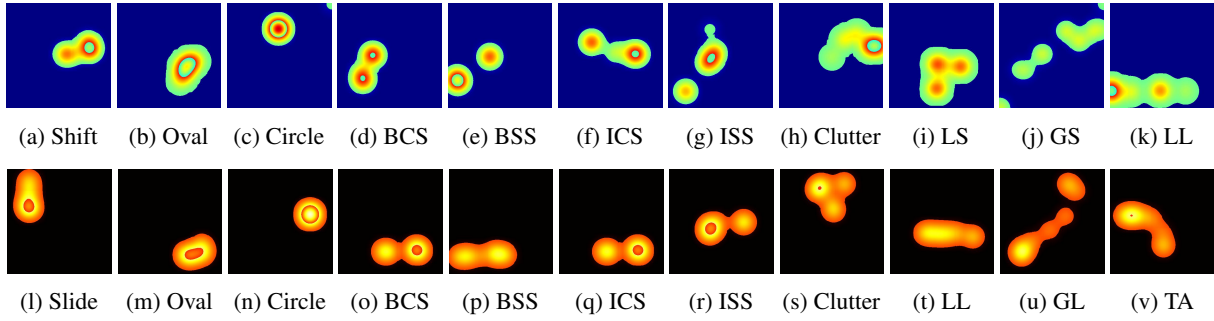


Figure 8: Heatmap visualizations of representative SBPs in Maze Painting across ASD and TD user groups from each discovered gaze [(a)-(k)] and touch [(l)-(v)] pattern category, where all the pattern categories are summarized in Table 2.

Table 2: Categorization of discovered SBPs and Wilcoxon rank sum test for each pattern category

Sensory	Shape	Pattern Category	P-value
Gaze	Concentrated	Shift	0.0985
		Oval	0.1042
		Circle	0.0965
	Switching	Balanced Clutter Switching (BCS)	0.0675
		Balanced Scatter Switching (BSS)	0.0876
		Imbalanced Clutter Switching (ICS)	0.0752
		Imbalanced Scatter Switching (ISS)	0.0923
	Local	Clutter	0.0623
		Local Scan (LS)	0.0518
	Global	Global Scan (GS)	0.0432
	Line	Local Line (LL)	0.0447
Touch	Concentrated	Slide	0.0802
		Oval	0.0857
		Circle	0.0968
	Switching	Balanced Clutter Switching (BCS)	0.0745
		Balanced Scatter Switching (BSS)	0.0736
		Imbalanced Clutter Switching (ICS)	0.0594
		Imbalanced Scatter Switching (ISS)	0.0654
	Local	Clutter	0.0518
		Turning Around (TA)	0.0485
	Line	Local Line (LL)	0.0469
		Global Line (GL)	0.0423

statistical results, we can claim that the local, global, and line patterns in the ASD and TD groups are significantly or near significantly different. This finding confirms our aforementioned statistical counts. The overall discovery is aligned with previous psychological studies that indicated adolescents with ASD are impaired in responding to stimuli that are subtle or complex (Wieckowski & White, 2020). Case studies on these ASD datasets are provided in Appendix F that uses the discovered SBPs to better understand

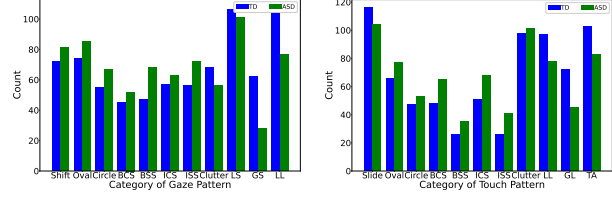


Figure 9: Gaze and touch SBP category statistical analysis autistic children's behaviors.

## 6. Conclusion

In this paper, we integrate deep temporal sets with evidential reinforced attention to discover subtle and complex multimodal human behavioral patterns. The proposed DTS-ERA model leverages two-tiered sequence encoders (*i.e.*, a temporal encoder and a spatial encoder) to generate DTS embedding that exploits temporal information. For effective model training, DTS-ERA uses the setting of few-shot learning that takes sampled sub-trajectories as the input tasks. By training across different tasks, the model can adapt to user data with different lengths to match real-world scenarios. Additionally, DTS-ERA combines an RL agent to perform evidential reinforced attention that learns an effective policy to select representative embeddings as attention signatures and further boosts the performance. Experimental results on multiple real-world datasets demonstrate the effectiveness of the proposed model. Signature behavioral patterns provide useful and interpretable insights to understand important behaviors that are unique for children with ASD.

---

## References

- 440 Amini, A., Schwarting, W., Soleimany, A., and Rus, D.  
441 Deep evidential regression. *Advances in Neural Information  
442 Processing Systems*, 33:14927–14937, 2020.
- 443
- 444
- 445 APA. *Diagnostic and statistical manual of mental disorders  
446 (5th ed.)*. American Psychological Association, 2013.
- 447
- 448 Babrak, L. M., Menetski, J., Rebhan, M., Nisato, G.,  
449 Zinggeler, M., Brasier, N., Baerenfaller, K., Brenzikofer,  
450 T., Baltzer, L., Vogler, C., et al. Traditional and digital  
451 biomarkers: two worlds apart? *Digital biomarkers*, 3(2):  
452 92–102, 2019.
- 453
- 454 Bai, S., Kolter, J. Z., and Koltun, V. An empirical evalua-  
455 tion of generic convolutional and recurrent networks for  
456 sequence modeling. *arXiv preprint arXiv:1803.01271*,  
457 2018.
- 458
- 459 Bent, B., Wang, K., Grzesiak, E., Jiang, C., Qi, Y., Jiang, Y.,  
460 Cho, P., Zingler, K., Ogbeye, F. I., Zhao, A., et al. The  
461 digital biomarker discovery pipeline: An open-source  
462 software platform for the development of digital biomark-  
463 ers using mhealth and wearables data. *Journal of clinical  
464 and translational science*, 5(1), 2021.
- 465
- 466 Bozgeyikli, L., Rajj, A., Katkoori, S., and Alqasemi, R. A  
467 survey on virtual reality for individuals with autism spec-  
468 trum disorder: design considerations. *IEEE Transactions  
469 on Learning Technologies*, 11(2):133–151, 2017.
- 470
- 471 Cai, Q., Wang, H., Li, Z., and Liu, X. A survey on multi-  
472 modal data-driven smart healthcare systems: approaches  
473 and applications. *IEEE Access*, 7:133583–133599, 2019.
- 474
- 475 Chen, K., Zhang, D., Yao, L., Guo, B., Yu, Z., and Liu,  
476 Y. Deep learning for sensor-based human activity recog-  
477 nition: Overview, challenges, and opportunities. *ACM  
478 Computing Surveys (CSUR)*, 54(4):1–40, 2021.
- 479
- 480 Crippa, A., Forti, S., Perego, P., and Molteni, M. Eye-hand  
481 coordination in children with high functioning autism  
482 and asperger’s disorder using a gap-overlap paradigm.  
483 *Journal of autism and developmental disorders*, 43:841–  
484 850, 2013.
- 485
- 486 Dempster, A., Schmidt, D. F., and Webb, G. I. MiniRocket:  
487 A very fast (almost) deterministic transform for time  
488 series classification. In *Proceedings of the 27th ACM  
489 SIGKDD Conference on Knowledge Discovery and Data  
490 Mining*, pp. 248–257, New York, 2021. ACM.
- 491
- 492 Elsayed, N., Maida, A. S., and Bayoumi, M. Deep gated  
493 recurrent and convolutional network hybrid model for  
494 univariate time series classification. *arXiv preprint  
495 arXiv:1812.07683*, 2018.
- 496
- 497 Fauvel, K., Lin, T., Masson, V., Fromont, É., and Ter-  
498 mier, A. XCM: an explainable convolutional neural net-  
499 work for multivariate time series classification. *CoRR*,  
500 abs/2009.04796, 2020. URL <https://arxiv.org/abs/2009.04796>.
- 501
- 502 Fauvel, K., Lin, T., Masson, V., Fromont, É., and Termier,  
503 A. Xcm: An explainable convolutional neural network  
504 for multivariate time series classification. *Mathematics*,  
505 9(23):3137, 2021.
- 506
- 507 Garnelo, M., Rosenbaum, D., Maddison, C., Ramalho, T.,  
508 Saxton, D., Shanahan, M., Teh, Y. W., Rezende, D., and  
509 Eslami, S. A. Conditional neural processes. In *Inter-  
510 national Conference on Machine Learning*, pp. 1704–1713.  
511 PMLR, 2018a.
- 512
- 513 Garnelo, M., Schwarz, J., Rosenbaum, D., Viola, F.,  
514 Rezende, D. J., Eslami, S., and Teh, Y. W. Neural pro-  
515 cesses. *arXiv preprint arXiv:1807.01622*, 2018b.
- 516
- 517 Gondal, M. W., Joshi, S., Rahaman, N., Bauer, S., Wuthrich,  
518 M., and Schölkopf, B. Function contrastive learning of  
519 transferable meta-representations. In *International Con-  
520 ference on Machine Learning*, pp. 3755–3765. PMLR,  
521 2021.
- 522
- 523 Gordon, J., Bronskill, J., Bauer, M., Nowozin, S., and  
524 Turner, R. E. Meta-learning probabilistic inference for  
525 prediction. *arXiv preprint arXiv:1805.09921*, 2018.
- 526
- 527 Hochreiter, S. and Schmidhuber, J. Long short-term memory.  
528 *Neural computation*, 9(8):1735–1780, 1997.
- 529
- 530 Ismail Fawaz, H., Lucas, B., Forestier, G., Pelletier, C.,  
531 Schmidt, D. F., Weber, J., Webb, G. I., Idoumghar, L.,  
532 Muller, P.-A., and Petitjean, F. Inceptiontime: Finding  
533 alexnet for time series classification. *Data Mining and  
534 Knowledge Discovery*, 34(6):1936–1962, 2020.
- 535
- 536 Karim, F., Majumdar, S., Darabi, H., and Chen, S. Lstm  
537 fully convolutional networks for time series classification.  
538 *IEEE access*, 6:1662–1669, 2017.
- 539
- 540 Kim, H., Mnih, A., Schwarz, J., Garnelo, M., Eslami, A.,  
541 Rosenbaum, D., Vinyals, O., and Teh, Y. W. Attentive  
542 neural processes. *arXiv preprint arXiv:1901.05761*, 2019.
- 543
- 544 Koirala, A., Yu, Z., Schiltz, H., Van Hecke, A., Armstrong,  
545 B., and Zheng, Z. A preliminary exploration of virtual  
546 reality-based visual and touch sensory processing assess-  
547 ment for adolescents with autism spectrum disorder. *IEEE  
548 Transactions on Neural Systems and Rehabilitation Engi-  
549 neering*, 29:619–628, 2021.
- 550
- 551 Le Glaz, A., Haralambous, Y., Kim-Dufor, D.-H., Lenca,  
552 P., Billot, R., Ryan, T. C., Marsh, J., Devylder, J., Wal-  
553 ter, M., Berrouiguet, S., et al. Machine learning and

- 495 natural language processing in mental health: systematic review. *Journal of Medical Internet Research*, 23(5): e15708, 2021.
- 496
- 497
- 498 Lee, K. F. A., Gan, W.-S., and Christopoulos, G. Biomarker-informed machine learning model of cognitive fatigue from a heart rate response perspective. *Sensors*, 21(11): 3843, 2021.
- 499
- 500
- 501
- 502
- 503 Lindor, E., Rinehart, N., and Fielding, J. Distractor inhibition in autism spectrum disorder: Evidence of a selective impairment for individuals with co-occurring motor difficulties. *Journal of Autism and Developmental Disorders*, 49:669–682, 2019.
- 504
- 505
- 506
- 507
- 508 Maenner, M. J., Shaw, K. A., Bakian, A. V., Bilder, D. A., Durkin, M. S., Esler, A., Furnier, S. M., Hallas, L., Hall-Lande, J., Hudson, A., et al. Prevalence and characteristics of autism spectrum disorder among children aged 8 years—autism and developmental disabilities monitoring network, 11 sites, united states, 2018. *MMWR Surveillance Summaries*, 70(11):1, 2021.
- 509
- 510
- 511 Mnih, V., Heess, N., Graves, A., and kavukcuoglu, k. Recurrent models of visual attention. In Ghahramani, Z., Welling, M., Cortes, C., Lawrence, N., and Weinberger, K. (eds.), *Advances in Neural Information Processing Systems*, volume 27. Curran Associates, Inc., 2014. URL <https://proceedings.neurips.cc/paper/2014/file/09c6c3783b4a70054da74f2538ed47c6-Paper.pdf>.
- 512
- 513
- 514
- 515
- 516 Noel, J.-P., De Niear, M. A., Lazzara, N. S., and Wallace, M. T. Uncoupling between multisensory temporal function and nonverbal turn-taking in autism spectrum disorder. *IEEE Transactions on Cognitive and Developmental Systems*, 10(4):973–982, 2017.
- 517
- 518
- 519
- 520
- 521
- 522
- 523
- 524
- 525
- 526
- 527
- 528
- 529
- 530
- 531
- 532
- 533
- 534
- 535
- 536
- 537
- 538
- 539
- 540
- 541
- 542
- 543
- 544
- 545
- 546
- 547
- 548
- 549
- 549 Paulus, R., Xiong, C., and Socher, R. A deep reinforced model for abstractive summarization. *CoRR*, abs/1705.04304, 2017. URL <http://arxiv.org/abs/1705.04304>.
- 549 Qin, S., Zhu, J., Qin, J., Wang, W., and Zhao, D. Recurrent attentive neural process for sequential data. *arXiv preprint arXiv:1910.09323*, 2019.
- 549 Sensoy, M., Kaplan, L., and Kandemir, M. Evidential deep learning to quantify classification uncertainty. *Advances in neural information processing systems*, 31, 2018.
- 549 Sutton, R. S., Barto, A. G., et al. Reinforcement learning. *Journal of Cognitive Neuroscience*, 1999.
- 549 Thieme, A., Belgrave, D., and Doherty, G. Machine learning in mental health: A systematic review of the hci literature to support the development of effective and implementable ml systems. *ACM Transactions on Computer-Human Interaction (TOCHI)*, 27(5):1–53, 2020.
- 549 Washington, P., Park, N., Srivastava, P., Voss, C., Kline, A., Varma, M., Tariq, Q., Kalantarian, H., Schwartz, J., Patnaik, R., et al. Data-driven diagnostics and the potential of mobile artificial intelligence for digital therapeutic phenotyping in computational psychiatry. *Biological Psychiatry: Cognitive Neuroscience and Neuroimaging*, 5(8): 759–769, 2020.
- 549 Wieckowski, A. T. and White, S. W. Attention modification to attenuate facial emotion recognition deficits in children with autism: A pilot study. *Journal of autism and developmental disorders*, 50(1):30–41, 2020.
- 549 Ye, J., Xue, Y., Long, L. R., Antani, S. K., Xue, Z., Cheng, K. C., and Huang, X. Synthetic sample selection via reinforcement learning. *CoRR*, abs/2008.11331, 2020.
- 549 Zaheer, M., Kottur, S., Ravanbakhsh, S., Poczos, B., Salakhutdinov, R. R., and Smola, A. J. Deep sets. *Advances in neural information processing systems*, 30, 2017.
- 549 Zeidan, J., Fombonne, E., Scorah, J., Ibrahim, A., Durkin, M. S., Saxena, S., Yusuf, A., Shih, A., and Elsabbagh, M. Global prevalence of autism: a systematic review update. *Autism Research*, 15(5):778–790, 2022.
- 549 Zou, X., Wang, Z., Li, Q., and Sheng, W. Integration of residual network and convolutional neural network along with various activation functions and global pooling for time series classification. *Neurocomputing*, 367:39–45, 2019. ISSN 0925-2312. doi: <https://doi.org/10.1016/j.neucom.2019.08.023>. URL <https://www.sciencedirect.com/science/article/pii/S0925231219311506>.

## Appendix

### Organization of Appendix

In Appendix A, we summarize the major notations used throughout the paper. In Appendix B, we provide additional details of the datasets and experimental setup. In Appendix C, we show the pseudo code of the training process. Appendix D provides the proofs of the main theoretical results. We present some additional experimental results in Appendix E and case studies in Appendix F. Appendix G discusses the limitations, future work, and social impact of the proposed work. Finally, the link to the source code and processed datasets is provided in Appendix H.

### A. Table of Symbols

The major notations and their descriptions are summarized in Table 3.

Table 3: Symbols with Descriptions

Notation	Description
$G$	Game Experience Collection
$\mathcal{T}_l^u, N_e$	Episode Trajectory for user $u$ in game level $l$ , variable length of episode trajectory
$\mathcal{T}^s, N_s$	Fixed size sub trajectory sampled from episode $\mathcal{T}$ as training input, length of input sub-trajectory $\mathcal{T}^s$
$\mathbf{t}_n, \mathbf{g}_n$	Instance level record in trajectory $\mathcal{T}$ (Instance)
$y, y_s$	User Category for episode trajectory $\mathcal{T}$ and sub-trajectory $\mathcal{T}^s$
$p$	padding size due to the kernel size of 1D-Conv layer.
$\{(h^1, \dots, h^{N_s})\}$	Multi-modality instance level record in input sub-trajectory $\mathcal{T}^s$
$\{(h_t^1, \dots, h_t^{N_s}), (h_s^1, \dots, h_s^{N_s})\}$	DTS module generated hidden embedding sets
$\mathbf{d}, \mathbf{d}_{attn}^t$	Average aggregated DTS module generated embedding and RL selected attentive subset embedding
$\mathbf{e}_t$	State Embedding representation
$\mathbf{s}_t$	State space representation in time step $t$
$\mathbf{a}_t, N_a$	Action space representation in time step $t$ and length of $\mathbf{a}_t$
$r^e(\mathbf{s}_t, \mathbf{a}_t)$	Evidential Reward associated with the state $\mathbf{s}_t$ and action $\mathbf{a}_t$
$r(\mathbf{s}_t, \mathbf{a}_t)$	Tradition Reward calculated by the last time step $T$ 's predictive accuracy.
$\gamma_{RL}$	Discounting factor used in the cumulative reward computation
$T$	length of RL time step in one training iteration
$P_T$	Last time step $T$ 's predictive result
$W$	Attention window length
$idx_t^k, k \in [1, N_a]$	Transform of each relative starting position $a_t^k$ to absolution position index in sub-trajectory $\mathcal{T}^s$ .
$\alpha, \beta, \nu, \gamma$	Output of evidential policy network to infer underlying Gaussian distribution.
$\mu, \sigma^2$	Mean and Variance of the inferred underlying Gaussian distribution for sampling action $\mathbf{a}_t$ .
$M_t$	Binary Attention Mask at time step $t$
$\pi_{\theta_e}, \theta_e$	evidential policy network and its parameter
$NN, \theta_{NN}$	binary classification network and its parameter
$(SE, \theta_{se})$	State Encoder and its parameter
$\Phi_t(\cdot), \Phi_s(\cdot)$	Temporal and Spatial Sequence Encoders
$\theta_d$	DTS module's joint parameter representation, including the parameter of Sequence and State Encoders.
$\eta_d, \eta_{NN}, \eta_e$	Learning rate of DTS module, classification network and evidential policy network.
$\lambda$	Hyper-parameter balancing the exploration and exploitation

## 605 B. Additional Details of Datasets and Experimental Setup

606 During the Maze Painting game, each participant finished 6 episodes in 2D scenario and another 6 episodes in 3D  
 607 scenario. To complete one episode, the participant had to completely paint the maze by operating a painting ball through  
 608 the Haptic robot. The trajectory of the ball, which reflected the applied touch sensation, was recorded at about 20Hz. In  
 609 addition, the participant's visual behavior was recorded as gaze position on the screen using a calibrated Tobii Pro x-30  
 610 eye-tracker at about 20-30 Hz. During the Word Scanning and Coloring games, each participant finished 6 episodes  
 611 in each game by operating the Haptic robot. The trajectory of the cursor (for word scanning) and the pen (for coloring),  
 612 which reflected the applied touch sensation, was recorded at about 60Hz. The participant's gaze position on the screen was  
 613 recorded by a calibrated Tobii Pro x-30 eye-tracker at about 20-25 Hz. Each user-episode data consists of a large number  
 614 of sequential records (one record represents the tracked gaze/touch data at a particular time) and its corresponding length  
 615 varied across the users and episodes. The tracked records were averaged across 0.1 second sequential intervals to obtain  
 616 the instances. Averaging over 0.1 second time interval reduced noise in the data and unified the vision and touch sampling  
 617 rates. Each gaze instance is a 4-dimensional feature vector indexed by time and represents the eye gaze position of each eye  
 618 on the screen. Each touch instance is a 3-dimensional feature vector indexed by time and represents the ball position on  
 619 the screen along with the applied pressure. During the data collection process, some users' behavior was not recorded due  
 620 to hardware/software issues, such as the participants blocking the view of the eye tracker or the robot controller having a  
 621 glitch. After removing these sections with incomplete data, we have a total of 100 2D user-episode combinations and 125  
 622 3D user-episode combinations, leading to a total of 225 user-episode combinations (termed mixed combination). For the  
 623 other two tasks (Word Scanning or Coloring), the number of user-episode combinations are both 132. We consider  
 624 60% of the available data (user episodes) of each sub-group (2D, 3D, mixed or word scanning, coloring) for training, train  
 625 the model for 2000 epochs, and evaluate the model on the remaining data in that sub-group. We repeat those experiments  
 626 across 5 random train-test splits and average the test set accuracy for quantitative evaluations.

## 627 C. Training Algorithm

628 In this section, we first derive the posterior predictive distribution of evidential policy network (i.e. Eq. 7) and then provide  
 629 the Algorithm 1 for detailed training process.

630 The evidential policy network is set up in such a way that the target, *i.e.*, action  $\mathbf{a}_t$ , is drawn i.i.d. from a Gaussian distribution  
 631 with unknown mean and variance  $(\mu, \sigma^2)$ . Model evidence can be introduced by further placing a prior distribution on  
 632  $(\mu, \sigma^2)$ . To ensure conjugacy, we choose a Gaussian prior on the unknown mean and an Inverse-Gamma prior on the  
 633 unknown variance:

$$634 p(\mathbf{a}_t|\mu, \sigma^2) = \mathcal{N}(\mu, \sigma^2) \quad (16)$$

$$635 p(\mu|\gamma, \sigma^2 \nu^{-1}) = \mathcal{N}(\gamma, \sigma^2 \nu^{-1}) \quad (17)$$

$$636 p(\sigma^2|\alpha, \beta) = \text{Inv-Gamma}(\alpha, \beta) \quad (18)$$

647 The joint posterior of  $(\mu, \sigma^2)$  can be formulated as a Normal Inverse-Gamma (NIG) distribution:  
 648

$$649 650 p(\mu, \sigma^2|\gamma, \nu, \alpha, \beta) = \frac{\beta^\alpha \sqrt{\nu}}{\Gamma(\alpha) \sqrt{2\pi\sigma^2}} \left( \frac{1}{\sigma^2} \right)^{\alpha+1} \exp \left\{ -\frac{2\beta + \nu(\gamma - \nu)^2}{2\sigma^2} \right\} \quad (19)$$

651 We can interpret the NIG distribution as a higher-order, evidential distribution, where the parameters of this distribution can  
 652 be interpreted as the (prior) pseudo-observations of an action. Our policy network directly predicts the NIG parameters,  
 653 which enables us to evaluate evidence for each action and measure epistemic uncertainty.

660 By marginalizing over  $(\mu, \sigma^2)$ , we arrive at the following predictive student-t distribution, which is used to sample actions:  
 661  
 662  
 663 
$$p(\mathbf{a}_t | \gamma, \nu, \alpha, \beta) = \int_{\sigma^2=0}^{\infty} \int_{\mu=-\infty}^{\infty} p(\mathbf{a}_t | \mu, \sigma^2) p(\mu, \sigma^2 | \gamma, \nu, \alpha, \beta) d\mu d\sigma^2$$
  
 664  
 665 
$$= \int_{\sigma^2=0}^{\infty} \int_{\mu=-\infty}^{\infty} \left[ \sqrt{\frac{1}{2\pi\sigma^2}} \exp\left\{-\frac{(a_t - \mu)^2}{2\sigma^2}\right\} \right] \left[ \frac{\beta^\alpha \sqrt{\nu}}{\Gamma(\alpha)\sqrt{2\pi\sigma^2}} \left(\frac{1}{\sigma^2}\right)^{\alpha+1} \exp\left\{-\frac{2\beta + \nu(\gamma - \mu)^2}{2\sigma^2}\right\} \right] d\mu d\sigma^2$$
  
 666  
 667  
 668 
$$= \int_{\sigma^2=0}^{\infty} \frac{\beta^\alpha \sigma^{-3-2\alpha}}{\sqrt{2\pi} \sqrt{1 + \frac{1}{\nu}\Gamma(\alpha)}} \left(\frac{1}{\sigma^2}\right)^{\alpha+1} \exp\left\{-\frac{2\beta + \frac{\nu(a_t - \mu)^2}{1+\nu}}{2\sigma^2}\right\} d\sigma^2$$
  
 669  
 670  
 671 
$$= \int_{\sigma=0}^{\infty} \frac{\beta^\alpha \sigma^{-3-2\alpha}}{\sqrt{2\pi} \sqrt{1 + \frac{1}{\nu}\Gamma(\alpha)}} \left(\frac{1}{\sigma^2}\right)^{\alpha+1} \exp\left\{-\frac{2\beta + \frac{\nu(a_t - \mu)^2}{1+\nu}}{2\sigma^2}\right\} 2\sigma d\sigma$$
  
 672  
 673  
 674 
$$= \frac{\Gamma(1/2 + \alpha)}{\Gamma(\alpha)} \sqrt{\frac{\nu}{\pi}} (2\beta(1 + \nu))^\alpha (\nu(a_t - \gamma)^2 + 2\beta(1 + \nu))^{-(\frac{1}{2} + \alpha)}$$
  
 675  
 676  
 677 
$$= \text{St}(\mathbf{a}_t; \gamma, \beta(1 + \nu)/(\nu\alpha), 2\alpha)$$

(20)

---

**Algorithm 1** Model Training

681 **Require:** Episode Trajectory  $\mathcal{T}$  of length  $N_e$  sampled from Game Experience Collection  $G = \{T_u^l\}, u \in U, l \in L$ , total  
 682 iteration number K, total time step T  
 683  
 684 **Require:** Hyperparameters:  $\eta_d$ ,  $\eta_{NN}$ , and  $\eta_e$  (learning rates),  $\gamma_{RL}$  (RL discount factor), evidential policy network  
 685 parameters  $(\theta_e)$ , Deep Temporal Sets module parameters  $(\theta_d)$ , and classification network parameters  $(\theta_{NN})$   
 686 **while** iteration k  $\leq$  K **do**  
 687     Randomly sample Episode Trajectory  $\mathcal{T}$  from Game Experience Collection and sample sub-trajectory  $\mathcal{T}^s$  of  $N_s$   
 688     instances from  $\mathcal{T}$   
 689     **for** time step t  $\in [1, T]$  **do**  
 690         Input sub trajectory  $\mathcal{T}^s$  into DTS module to generate gaze and touch representation as (3).  
 691         Concatenate DTS module generated embeddings and RL-agent selected attentive regions as in (5).  
 692         Input  $e_t$  into state encoder as equation (6) to generate current state  $s_t$   
 693         Input state  $s_t$  into evidnetial policy network to get action  $a_t$ , and calculate evidential reward  $r^e(s_t, a_t)$  using equation  
 694         (9) in the last time step T  
 695         Pass  $s_t$  to classification network to get final prediction  $p_T$  and update the network as (13)  
 696     **end for**  
 697     Update evidental policy network as (15) and DTS module as (12) respectively  
 698     **end while**

---

**D. Proofs of Theoretical Results**

701 In this section, we provide proofs of all lemmas and the theorem.

**D.1. Proof of Lemma 1**

706 Given the evidential reward defined as  $r^e(s_t) = r_\pi(s_t) + \lambda_{\text{epistemic}}(\cdot | s_t)$  the update rule for epistemic value can be  
 707 written as:

708  
 709 
$$V^e(s_t) = \mathbb{E}_\pi \sum_{t'=t}^{\infty} \gamma^{t'} r^e(s_{t'}) = r^e(s_t) + \gamma \mathbb{E}_{s_{t+1}}[V^e(s_{t+1})]$$

(21)

712 Following the convergence rule (Sutton et al., 1999) with finite action space, it is guaranteed that the value will converge to  
 713 the epistemic value of policy  $\pi$ .

## D.2. Proof of Lemma 2

The policy can be updated towards the new value function. Consider the updated policy  $\pi_{new}$  as the optimizer of the maximization problem.

$$\pi_{new} = \arg \max_{\pi'} J_{\pi}(\phi) = \arg \max_{\pi'} \mathbb{E}_{\mathbf{s}_t} [V_{\pi'}^e(\mathbf{s}_t)] \quad (22)$$

Denote the old policy as  $\pi_{old}$ . Using the update rule specified in Eq (15) with a sufficiently small step size, we get an updated policy  $\pi_{new}$  that satisfies

$$\mathbb{E}_{\mathbf{a}_t \sim \pi_{new}} [V_{\pi_{old}}^e(\mathbf{s}_t)] \geq \mathbb{E}_{\mathbf{a}_t \sim \pi_{old}} [V_{\pi_{old}}^e(\mathbf{s}_t)] \quad (23)$$

Given Eq (23), we have the following inequality

$$\begin{aligned} V_{\pi_{old}}^e(\mathbf{s}_t) &\leq r^e(\mathbf{s}_t) + \gamma \mathbb{E}_{\mathbf{s}_{t+1}, \mathbf{a}_{t+1} \sim \pi_{new}} [V_{\pi_{old}}^e(\mathbf{s}_{t+1})] \\ &\leq r^e(\mathbf{s}_t) + \gamma \mathbb{E}_{\mathbf{s}_{t+1}, \mathbf{a}_{t+1} \sim \pi_{new}} [r^e(\mathbf{s}_{t+1})] \\ &\quad + \mathbb{E}_{\mathbf{s}_{t+2}, \mathbf{a}_{t+2} \sim \pi_{new}} [V_{\pi_{old}}^e(\mathbf{s}_{t+2})] \\ &\dots \\ &= V_{\pi_{new}}^e(\mathbf{s}_t) \end{aligned} \quad (24)$$

where  $r^e(\mathbf{s}_t)$  is a evidential reward in step  $t$ . Therefore, we show that the new policy  $\pi_{new}$  ensures  $V_{\pi_{new}}^e(\mathbf{s}_t) \geq V_{\pi_{old}}^e(\mathbf{s}_t)$  for all  $\mathbf{s}_t$ .

## D.3. Proof of Theorem 3

Let  $\pi_i$  denote the policy at iteration  $i$ . We already show that the sequence  $V_{\pi_i}^e(\mathbf{s}_t)$  is monotonically increasing. Since  $V_{\pi}^e(\mathbf{s}_t)$  is bounded above, the sequence converges to some  $\pi^*$ . At convergence, it must be the case that  $J_{\pi^*}(\pi^*(\cdot | \mathbf{s}_t)) \leq J_{\pi^*}(\pi(\cdot | \mathbf{s}_t))$  for  $\pi \neq \pi^*$ . Based on Lamma 2, we have  $V_{\pi^*}^e(\mathbf{s}_t) > V_{\pi}^e(\mathbf{s}_t)$  for all  $\mathbf{s}$ . In other words, the evidence value of any other policy  $\pi$  is lower than that of the converged policy  $\pi^*$ . Therefore, it guarantees convergency to an optimal policy  $\pi^*$  such that:

$$V_{\pi^*}^e(\mathbf{s}_t) \geq V_{\pi}^e(\mathbf{s}_t) \quad (25)$$

## E. Additional Experiment Results

### E.1. Ablation study on hyper-parameters

Figure 10 presents the impact of different hyper-parameters: dimensionality of DTS embedding, length of the input sub-trajectory  $N_s$ , and length of RL time step  $T$  in one training iteration. Specifically, when embedding's latent dimensionality is set to 256, input sub-trajectory length is set to 60, and RL time step is set to 5, our model achieves the best performance.

### E.2. Additional Result on Incomplete Trajectories

Figure 11 shows DTS-ERA's performance by taking 20%, 40%, 60%, 80% and whole trajectory on the mixed dataset (*i.e.*, 2D+3D). This result is consistent with the results shown in the main paper, which further demonstrates our model's good detection performance using only partial trajectories.

### E.3. Visualization of DTS-ERA Embedding

To provide additional insights on the outstanding detection performance of the proposed model, we project the learning DTS-ERA selected attentive subset embedding into a low-dimensional space and visualize the testing trajectories in Figure 12. We leverage PCA to further reduce the dimensionality of attentive subset embeddings and choose two principle components to visualize the trajectories (each is mapped to a point in the 2d space). As can be seen, the TD and ASD groups become easily separated even in such a low-dimensional space.

## F. Case Study

We conducted a case study in both 2D and 3D Maze game environments by collecting autistic and TD users' most frequent gaze and touch SBPs in game levels 6 and 11, respectively. Level 6 was a 2D game environment with a cube distractor

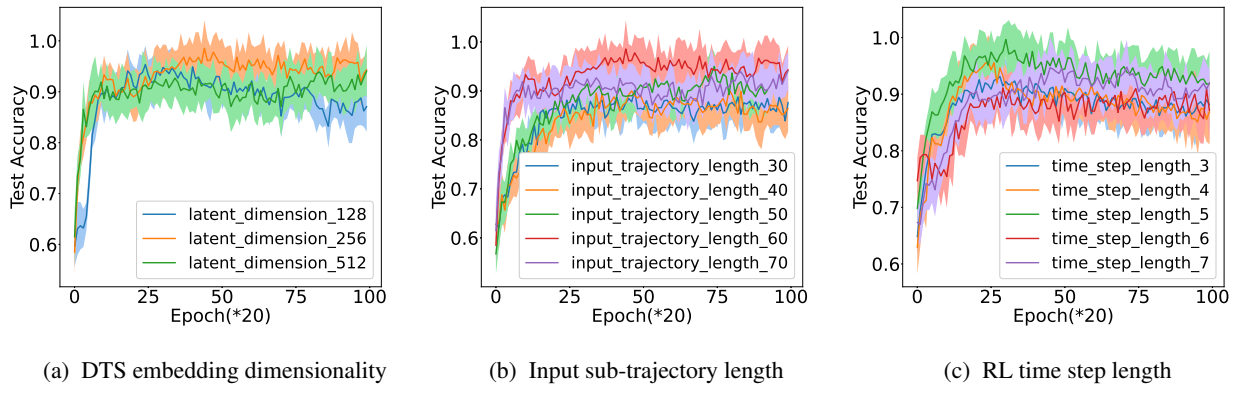


Figure 10: Impact of hyper-parameters

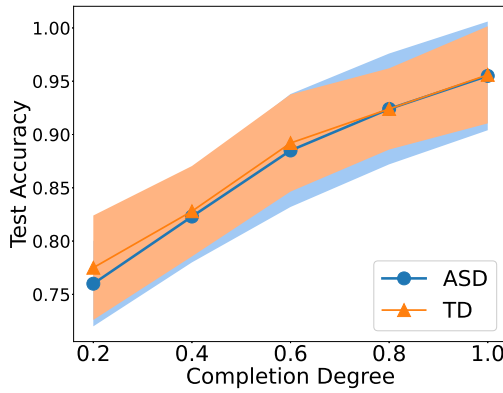


Figure 11: Incomplete Data [Mixed]

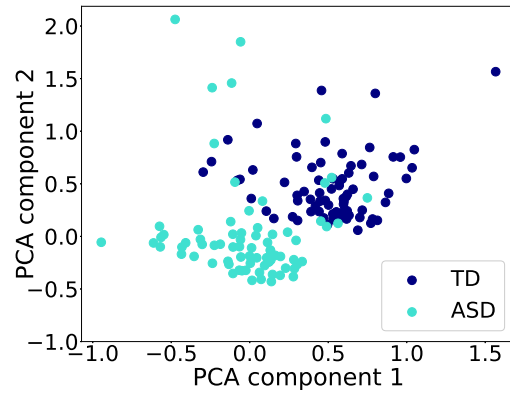


Figure 12: Visualizing the DTS-ERA embedding

located in the middle; Level 11 was a 3D environment where distractors spread across the board. The result is shown in Figure 13. In the 2D environment of game level 6 (the first row), both groups' gaze and touch followed a line shape in most cases. The difference was that TD users' line spread longer and more diverse than that of the autistic users, thus forming long-range and curve patterns, such as Global Scan (GS) and Global Line (GL), as compared to autistic users' Local Line (LL) and Shift patterns for gaze and touch. This observation is also consistent with the 3D environment (the second row), where the ASD users' most frequent gaze and touch SBPs were both concentrated patterns. In contrast, the TD users show Local Scan (LS) and Turning Around (TA) patterns for gaze and touch, respectively. We combined 2D and 3D observations and analyze them jointly and found an interesting phenomenon for autistic users: they tended to look at and move the ball along the math path near the margin of the gaming scene. More importantly, their eye gaze and ball movement in most cases were in the opposite positions, as shown in Figures 13a and 13b as well as 13f and 13g. These were the most frequent gaze and touch patterns of the ASD group in 2D and 3D environments. This finding is aligned with previous child development research that showed children with ASD tend to demonstrate less efficient eye-hand coordination (Crippa et al., 2013). In the 3D environment, autistic users' eye gaze patterns fell more on the cube distractors, shown in Figure 13f. They pushed the ball harder as indicated by brightness in Figure 13g but with little movement. In contrast, the TD users usually scanned more widely beyond the distractors and continue to move the ball along the path near the distractors to complete the painting task, as shown in Figures 13h and 13i. Such observations coincided with our statistical analysis and provided evidences that support previous research about the potential ASD related impairment in distractor inhibition (Lindor et al., 2019).

Given the simpler gaming operations in Word Scanning and Coloring, the SBPs found on those tasks are rather simple. Both ASD and TD groups demonstrated a certain level of consistency between touch and gaze modalities, while autistic children's gaze and touch locations seem more separated than the TD group. TD users' gaze and touch patterns were more likely to show (global) line, curve or (local) clutter patterns, while the ASD group tended to show more localized

patterns, such as **concentrated** and **switching**. We choose one most frequent gaze or touch SBPs in Word Scanning and Coloring tasks respectively to demonstrate this finding, shown as Figure 14.

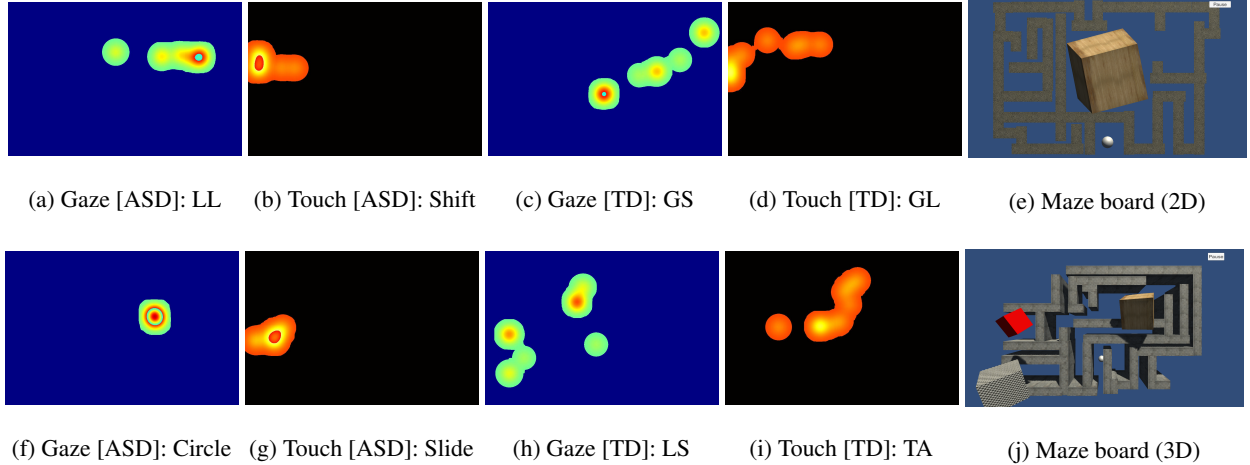


Figure 13: (a)-(d): gaze and touch SBPs for ASD and TD users in game level 6 (2D-environment); (f)-(j) gaze and touch SBPs for ASD and TD users in game level 11 (3D-environment); (e) and (j) maze boards for 2D and 3D environments

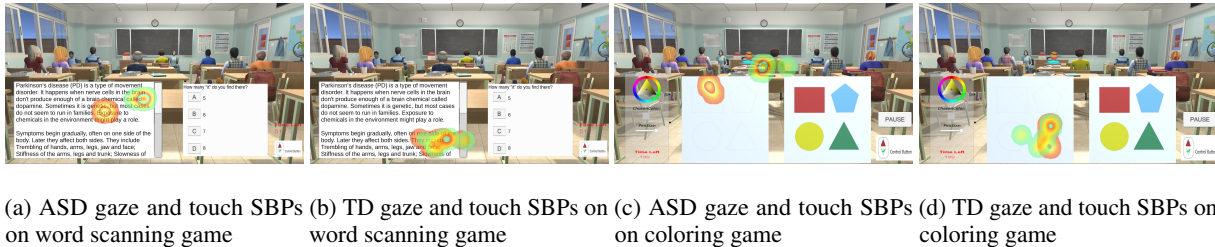


Figure 14: SBPs visualization for word scanning and coloring games

## G. Limitations, Future Work, and Social Impact

While the proposed new DTS-ERA model presents a general method for complex behavioral pattern discovery, our evaluation focuses on ASD-related behavior detection using datasets collected from child-computer interaction. Nevertheless, the model evaluation methodology can be adapted to other datasets and baseline algorithms in a broader context. It is worth to note that the current datasets have missing data, which is a common issue in real-world scenarios due to human and device limitations. Thanks to the few-shot training approaches, our model still achieves robust prediction performance. The current discoveries emphasize potential applications of the model for ASD assessment. This is a starting point for future extensions of our framework: leverage machine learning technology to help improve human behavioral pattern discovery in real-world applications, such as mental/behavioral health care. As a next step, we will utilize more diverse and longer-time human behavior data within and beyond the ASD field to further explore real-world challenges and adapt the proposed model to more complex settings. The proposed DTS-ERA model is generally applicable to many sequential decision-making real-world problems such as healthcare, robotics, and gaming domains. For instance, the model could potentially be used for preliminary screening before expert (such as healthcare professionals) validation, which may speed up disease diagnosis and provide patients with prompt and effective treatment. Moreover, our model could also be used for digital behavior biomarker detection and digital behavioral phenotyping to better understand the behavioral/sensory patterns of individuals with mental and/or behavioral issues. These will further advance diagnosis and treatment.

## H. Source Code

The source code and processed datasets can be accessed here: [https://anonymous.4open.science/r/ASD\\_TD-8B4C/README.md](https://anonymous.4open.science/r/ASD_TD-8B4C/README.md)